

# RSC Advances



This is an *Accepted Manuscript*, which has been through the Royal Society of Chemistry peer review process and has been accepted for publication.

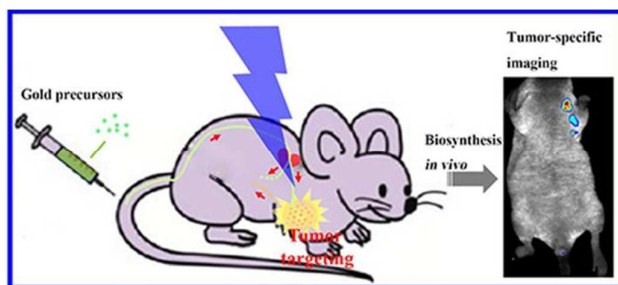
*Accepted Manuscripts* are published online shortly after acceptance, before technical editing, formatting and proof reading. Using this free service, authors can make their results available to the community, in citable form, before we publish the edited article. This *Accepted Manuscript* will be replaced by the edited, formatted and paginated article as soon as this is available.

You can find more information about *Accepted Manuscripts* in the [Information for Authors](#).

Please note that technical editing may introduce minor changes to the text and/or graphics, which may alter content. The journal's standard [Terms & Conditions](#) and the [Ethical guidelines](#) still apply. In no event shall the Royal Society of Chemistry be held responsible for any errors or omissions in this *Accepted Manuscript* or any consequences arising from the use of any information it contains.

### Graphical Abstract

*In vivo* simultaneous and multisite tumor rapid-targeting through specifically biosynthesized gold nanoclusters could be readily followed and monitored by real-time fluorescence imaging.



Cite this: DOI: 10.1039/c0xx00000x

www.rsc.org/xxxxxx

ARTICLE TYPE

# Simultaneous and multisite tumor rapid-target bioimaging through biosynthesis *in vivo* of fluorescent gold nanoclusters

Jianling Wang<sup>a</sup>, Jing Ye<sup>a</sup>, Hui Jiang<sup>a</sup>, Shengping Gao<sup>a</sup>, Wei Ge<sup>a</sup>, Yun Chen<sup>a</sup>, Chongyang Liu<sup>c</sup>, Christian Amatore<sup>b</sup>, Xuemei Wang<sup>\*a</sup>

Received (in XXX, XXX) Xth XXXXXXXXX 200X, Accepted Xth XXXXXXXXX 200X

DOI: 10.1039/b000000x

**Abstract:** Simultaneous and multisite tumor rapid-target bioimaging has been realized in this contribution through biosynthesis *in vivo* of fluorescent gold nanoclusters (GNCs). The selectively biosynthesized fluorescent GNCs in cancer cells or tumor tissues by systemic bio-administration of gold precursors via tail vein injection in tumor bearing mice were found to exhibit highly efficient tumor targeting effect. Intracellular fluorescence study demonstrates that *in vivo* biosynthesized GNCs from cancer cells could efficiently label and image target cells with bright photostable fluorescence, which could be readily exploited for the rapidly imaging *in vivo* the biodistribution of GNCs in mice and thus efficiently determine the precise target sites of fluorescent GNCs specifically biosynthesized in tumor tissues with high spatiotemporal resolution. Moreover, histopathologic analyses of H&E-stained tissue sections indicate that no side effects for mice treated with gold precursors are found during the process of systemic bio-administration for gold precursors. This raises the possibility of utilizing the *in vivo* biosynthesized GNCs through intravenous administration of biocompatible gold precursors as promising and effective biomarkers for rapid tumor diagnosis and precisely surgical intervention.

## 1. Introduction

Molecular clusters of pure metals, especially noble metals (i.e., gold, silver or platinum), due to their inert reactivity and biocompatibility, are attracting a wealth of attention in biomedicine. These ultrasmall particles with finite cluster size, termed nanoclusters, present molecular-like electronic transitions between HOMO-LUMO energy levels.<sup>1,2</sup> Besides the unique electronic nature of gold-based nanocomposites, intriguing physical and chemical properties are promising in these nanomaterials, and obtain new opportunities for optical and biomedical applications,<sup>3-6</sup> including imaging, biosensing, diagnostics, and therapy.<sup>7,8</sup> Recent research indicates that nanoparticle-based imaging could be used for molecular imaging of tumor microenvironment and image-guided interventions including drug delivery, surgery and ablation therapy, especially fluorescence GNCs, exhibit a great potential for the tumor target imaging *in vitro* and *in vivo*.<sup>9,10</sup> It is noted that various nanoclusters, especially GNCs protected by biomolecules (e. i. glutathione, bovine serum albumin, DNA), are favoured as bioprobes for tumor target imaging in biomedical field.<sup>11-14</sup> Generally, GNCs can biodegrade into subunits to facilitate rapid excretion, reducing the potential for toxicity.<sup>15</sup> More interestingly, some multifunctional gold nanoparticles with good biocompatibility could be prepared by using a biological or

microbiological system as a potential “nanofactory”, through a biomineralization synthetic route. The exposure of the fungus *werticillium sp.* to an aqueous solution of AuCl<sub>4</sub><sup>-</sup> resulted in the reduction of the salt to gold nanoparticles scattering on the cell surface as well as intracellularly with uniform size.<sup>16,17</sup> *In situ* biosynthesis of gold NCs could be also readily realized through employing the peculiarities of cancer cells or tumor tissues.<sup>18</sup> Our observations demonstrate that *in situ* biosynthesized gold NCs from cancer cells mainly presents the valence of gold atoms, ranged between 2-3 nm in diameter with the steady-state fluorescence spectrum. Although the mechanism of the biosynthesis of the NCs in these biological systems is immature or even unknown, presumably, different biosynthetic products such as reduced cofactors play an important role in the reduction of the gold precursor to the GNCs. In this contribution, we have found that the biocompatible, fluorescent GNCs could be selectively biosynthesized in cancer cells or tumor tissues by systemic bio-administration of gold precursors, and simultaneously exhibit highly efficient tumor targeting, with extremely bright and photostable emission in cancer cells and tumor bearing mice (Fig. 1), to effectively improve the precision of cancer diagnosis and therapy.

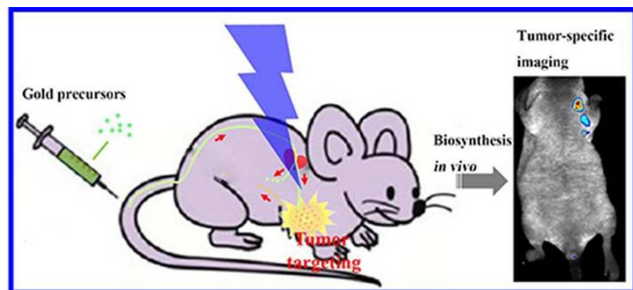


**Fig. 1** Scheme of tumor targeting of metabolizable probes. *In vivo* tumor targeting through specifically biosynthesized gold NCs could be readily followed by fluorescence imaging in real time after intravenous injection of chlorauric acid prepared in PBS into nude mice, evidencing the ability of rapid and specific tumor targeting through biosynthesized fluorescent nanoclusters in tumors to efficiently and precisely bioimage regions of tumors *in vivo*.

## 2. Experimental

### 2.1. Cell culture and tumor model

HeLa cells (kindly provided by Professor Chongyang Liu in Third Military Medical University) were cultured and maintained in Dulbecco's modified Eagle's medium (DMEM), supplemented with 10% fetal bovine serum (FBS), 1% penicillin/streptomycin at 37 °C, 5% CO<sub>2</sub> and a 95% humidified atmosphere.

Approximately 4-week old female BALB/c athymic nude mice (Peking University Health Science Center) were maintained in accordance with the National Institute of Biological Science and Animal Care Research Advisory Committee of Southeast University, while experiments conducted following the guidelines of the Animal Research Ethics Board of Southeast University. BALB/c nude mice were implanted subcutaneously with HeLa cells ( $2 \times 10^6$  cells in 0.1 mL PBS) in the left armpit. The day of tumor cell implantation was defined as day 0. On the tenth day after implantation of the tumor cell, tumors were grown until the dimension was approximately 7 mm.

### 2.2. Transmission electron microscopy

The HeLa cells of a whole culture flask incubated with 10  $\mu\text{mol/L}$  AuCl<sub>4</sub><sup>-</sup> solution prepared in PBS for 24 or 48 h at 37 °C, 5% CO<sub>2</sub>. The cells were detached with a cell scraper, dispersed in PBS, centrifuged the mixture at 1000 rpm for 5 min., and fixed in 1% glutaraldehyde in PBS. After fixation in 1% osmium tetroxide, the cells were dehydrated in graded series of acetone and infiltrated and embedded in Araldite 502 and polymerized at 60 °C for 3 days. Ultrathin sections (70 nm thick) were cut using a diamond knife (Diatome) in Leica Ultracut UCT microtome and were taken up on 300 mesh copper grids. Thereafter, the grids with the sections were stained with uranyl acetate and lead citrate and were viewed with a transmission electron microscope (Hitachi TEM system, HC-1) at an accelerating voltage of 80 kV. A JEM-2100 transmission electron microscope (TEM) was used to characterize the size and size distribution of biosynthesized GNCs in HeLa cells, which were obtained from the cells by a repetitive freeze-thaw method from -20 °C to 37 °C. The procedures used to extract gold nanoclusters from cells were elaborated as follows: Firstly, the HeLa cells incubated with 10  $\mu\text{mol/L}$  AuCl<sub>4</sub><sup>-</sup> solution were trypsinized and harvested in

Eppendorf tubes, and then dispersed with PBS, centrifuged at 1000 rpm for 5 min, and collected in Eppendorf tubes. Afterwards, the collected cells were re-dispersed in 2 mL Milli-Q water for extracting the gold nanoclusters from these HeLa cells by a frequently repetitive freeze-thaw method from -20 °C to 37 °C for ~5 h. Lastly, the mixture was centrifuged at 1500 rpm for 3 min, and the supernatant with gold nanoclusters were collected.

### 2.3. *In vivo* bio-imaging study

For cellular imaging, HeLa cells were treated with AuCl<sub>4</sub><sup>-</sup> solutions and incubated at 37 °C for 12, 24 or 48 h. The cells were washed three times with PBS before fluorescence imaging. A 488-nm excitation laser beam (Andor Revolution XD) was focused using a 20  $\times$  IR coated objective (Nikon).

For *in vivo* bio-imaging of gold nanoclusters in the tumor location, the xenograft tumor mice received an administration of 10 mmol/L AuCl<sub>4</sub><sup>-</sup> solution prepared in PBS (100  $\mu\text{L}$ ) via tail vein injection. The mice were fully anesthetized by inhalation of a mixture of oxygen with 5% isoflurane at times of 2, 8, 12, 24, and 48 h post-injection. The *in vivo* bio-images were acquired on Cri Maestro *in vivo* imaging system (excitation: ~455 nm, emission: 570-780 nm). The ROI (regions of interest) analysis was measured under the assistance of CRi Maestro Image software. The studies were approved by the National Institute of Biological Science and Animal Care Research Advisory Committee of Southeast University, while experiments conducted following the guidelines of the Animal Research Ethics Board of Southeast University.

### 2.4. Quantitation of gold species uptake by tumor and biodistribution by ICP-MS

The tumor uptakes and biodistribution of gold contents were determined by using inductively coupled plasma mass spectrometry (ICP-MS). After finishing the experiments of *in vivo* imaging at 48 h post-injection, the mice were sacrificed. Both tumors and important organs/tissues such as heart, liver, spleen, lung, kidney, intestines, brain, and skin were harvested, and were thoroughly washed with phosphate buffered saline (PBS) and blotted dry to minimize the contribution of any contaminants. Uptake and biodistribution of gold contents by tumor and tissues/organs were determined by using ICP-MS after they were eroded by HNO<sub>3</sub> and H<sub>2</sub>O<sub>2</sub>.

### 2.5. Histopathologic analyses of tissues

The livers, spleens, and kidneys were extracted from HeLa tumor-bearing mice and fixed in a 4% paraformaldehyde solution. The organs were embedded in paraffin, sectioned, and stained with hematoxylin and eosin (H&E). The images were obtained by using a BX53 microscopy system (Olympus, Tokyo, Japan) that was equipped with a color CCD (DMK 41BU02, Sony Co., Tokyo, Japan).

## 3. Results and discussion

### 3.1. Characterization of biosynthesized gold NCs for cellular imaging

In this research, HeLa cells was selected as model to biosynthesize gold NCs and to evaluate the tumor targeting efficiency of these biosynthesized gold NCs. As shown in Fig. 2, when HeLa cells incubated with chloroauric acid solution, transmission electron microscopy (TEM) images of the microtomed specimens clearly illustrated the structures of whole cells, including cytomembrane and nuclear membrane keep intact. The gold NCs keeps monodisperse without any aggregation in the whole cells, which agrees well with the good performance of the fluorescent gold NCs (Fig. 3 and Fig. 4). The present biosynthesized gold nanoclusters display the same typical UV/Vis absorption spectrum as observed for chemically prepared gold nanoclusters (Fig. 3), which agrees the UV/Vis spectrum of chemically prepared gold nanoclusters<sup>19</sup>. In addition, the fluorescence of gold nanoclusters biosynthesized *in situ* could be observed clearly (Fig.3), which corresponded with the steady-state fluorescence spectrum of gold nanoclusters in aqueous solution with an emission peak at ca. 580 nm.

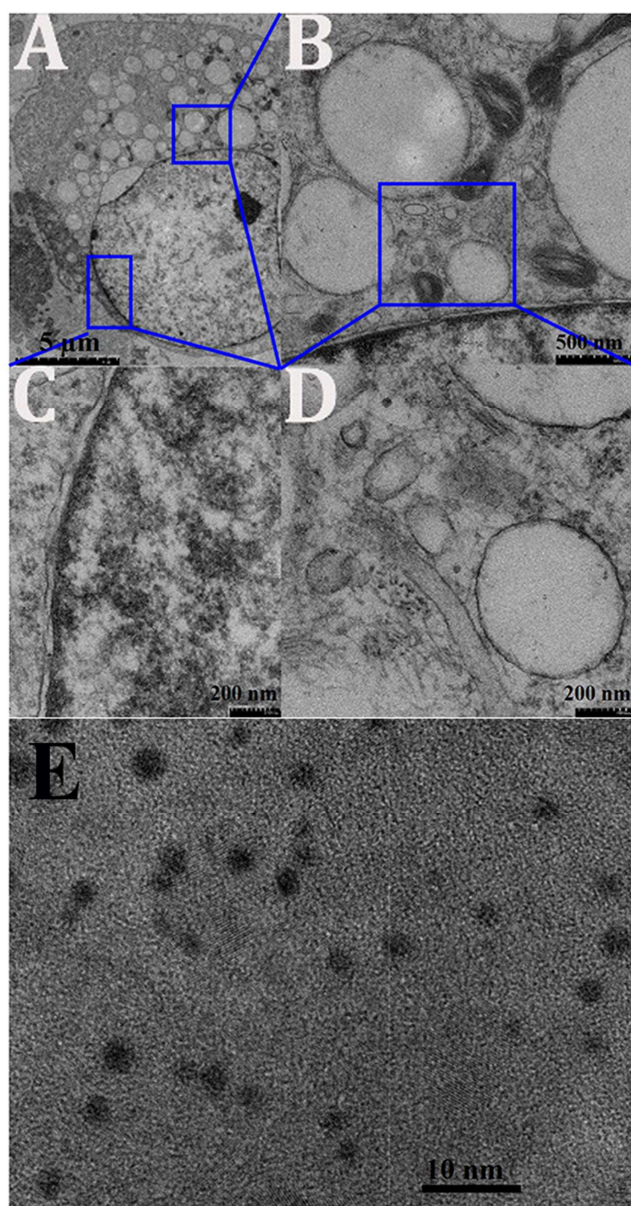


**Fig.2.** Transmission electron microscopy (TEM) of HeLa cells after incubation with 10  $\mu\text{mol/L}$   $\text{AuCl}_4^-$  and biosynthesis of gold NCs. (A) Panoramic images of HeLa cells with the *in situ* biosynthesized gold NCs; the regions in the boxes of (A) are enlarged in (B and C); the region in the box of (B) is further enlarged in (D). (E) TEM image of the gold NCs extracted from incubated HeLa cells shows that the mean size of the gold NCs is around  $1.8 \pm 0.3$  nm, with a rather uniform size distribution.

Fig. 4 demonstrates the typical images of laser-scanning confocal fluorescence microscopy of the gold NCs biosynthesized in HeLa cells. As determined by confocal fluorescence imaging, HeLa cells incubated with  $\text{AuCl}_4^-$  solution (10  $\mu\text{M}$ ) for 12 h showed only a weak green fluorescent emission (Fig. 4 (B)). When the cells were incubated with  $\text{AuCl}_4^-$  solution (10  $\mu\text{M}$ ) for longer time (i. e. 24 or 48 h), a strong enhancement in the green fluorescent emission was observed in the intracellular region (Fig. 4 (C, D)).

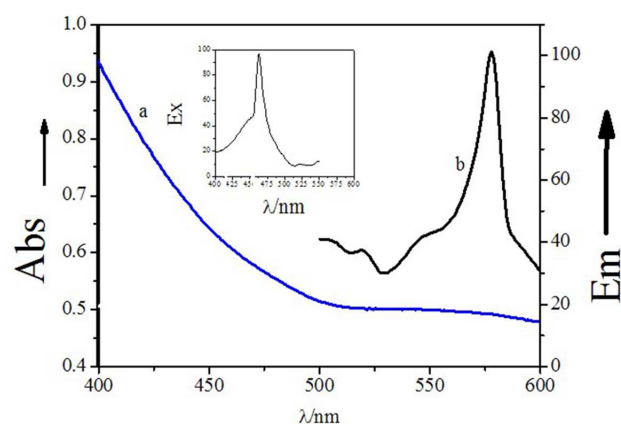


**Fig. 3.** Optical characterization of the gold nanoclusters extracted from incubated HeLa cells. Curve a shows the UV/Vis absorption spectrum of the relevant gold nanoclusters; curve b shows their fluorescence emission spectrum (Em) at a 575 nm excitation wavelength (their excitation spectrum (Ex) is shown in the inset).

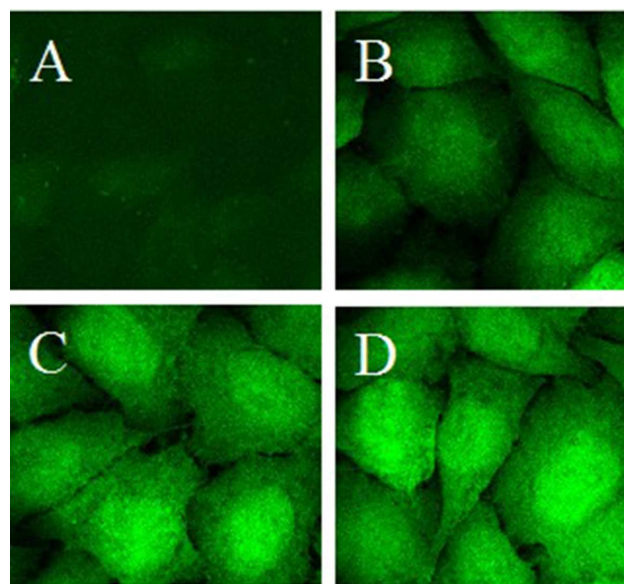


**Fig.4.** Laser confocal fluorescence micrographs of HeLa cells incubated with identical 10  $\mu\text{mol/L}$   $\text{AuCl}_4^-$  solution prepared in PBS for different times. A: 0 h; B: 12 h; C: 24 h; D: 48 h. Images were acquired at 400-fold

magnification.

### 3.2. Simultaneous and multisite *in vivo* tumor rapid-target bioimaging

Simultaneous and multisite tumor rapid-target bioimaging has been further realized in this study through biosynthesis *in vivo* of fluorescent gold NCs. As shown in Fig. 5-I, it is evident that the fluorescent gold NCs can only be spontaneously produced in tumor sites of HeLa tumor-bearing mice, while the fluorescence signal can hardly be observed in normal mice under the same conditions. It is noteworthy that the fluorescence signal can be simultaneously observed at three independent tumor sites, and, meanwhile, the fluorescence intensity increases with longer time after injection (Fig. 5). Noticeably, it is observed that the rapid and precise bio-imaging of the target tumors could be readily realized in less than 2h through the specifically biosynthesized gold NCs *in vivo* after the intravenous injection of gold precursors through the tail of mice, evidencing the ability of rapid and specific tumor targeting through *in vivo* biosynthesized fluorescent nanoclusters to efficiently facilitate simultaneous and multisite bioimaging of the precise tumor regions. Most interestingly, the fluorescence signal can be observed in urethra at 48 h (Fig. 5-I-C), indicating that these gold species, ultrasmall fluorescent gold NCs, can be metabolized and cleared from the body through kidney filtration.

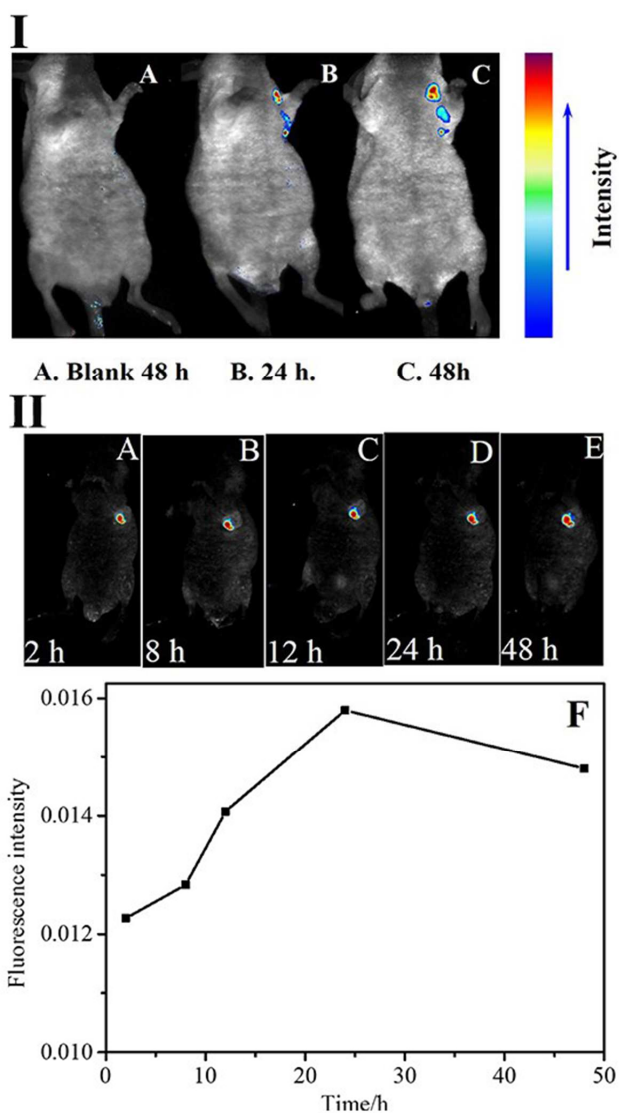


**Fig.5.** Fluorescence imaging of BALB/c mice at various time points post tail-vein injection of 0.1 mL 10 mmol/L  $\text{AuCl}_4^-$  solution prepared in PBS. All images were acquired under the same instrumental parameters. Representative xenograft tumor mouse models of HeLa carcinoma (I-B and I-C) observed by *in vivo* fluorescence imaging after an injection of 0.1 mL 10 mmol/L  $\text{AuCl}_4^-$  solution. I-A: Normal mouse 48 h; I-B: 24 h; I-C: 48 h. (II): *In vivo* images of tumor bearing mice at various time points (2, 8, 12, 24, 48 h). II-F: The variations of mean fluorescence intensity at various time points.

On the basis of the above observations, we have further explored the tumor-specific targeting ability of the biosynthesized gold NCs as well as the biodistribution of gold contents. Initially, tumors and important organs/tissues such as heart, liver, spleen, lung, kidney, intestines, brain, and skin were harvested from HeLa tumor-bearing mice with intravenous administration of 0.1 mL 10 mmol/L  $\text{AuCl}_4^-$  solution prepared in PBS at 48 h post-injection. Then gold contents in the tumor tissue and different organs/tissues were investigated by ICP-MS techniques. The uptakes of gold species on tumor tissues, as shown in Fig. 6, are generally well in consistency with the relevant imaging observed in Fig. 5, suggesting that the gold species prefer to accumulate on tumor tissues due to the particularity of tumor tissues or tumor

microenvironments. For the biodistribution of gold contents in 48 h after the initial injection, the highest gold levels were found in the kidney and spleen, whereas the lowest levels were found in the brain. Moderate gold levels were found in the liver, lung, and skin. In addition, it can be found that in heart and intestines Au concentration is of ~0.80% and ~0.86%, respectively.

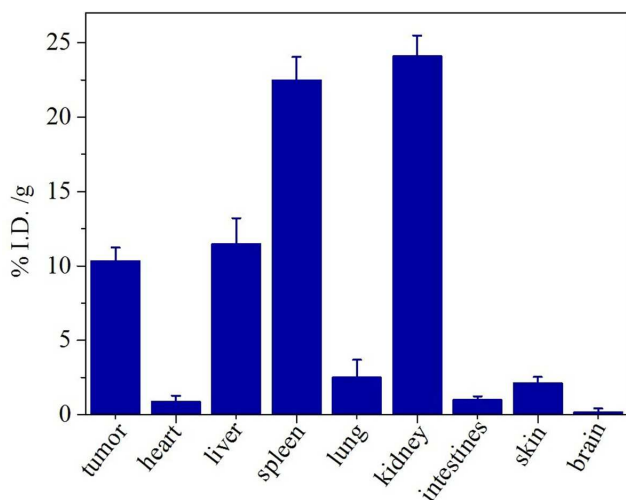


**Fig. 6.** Gold content in various organs or tissues of HeLa tumor-bearing mice with injection of 100  $\mu\text{L}$  10 mmol/L  $\text{AuCl}_4^-$  solution prepared in PBS at 48 h post-injection.

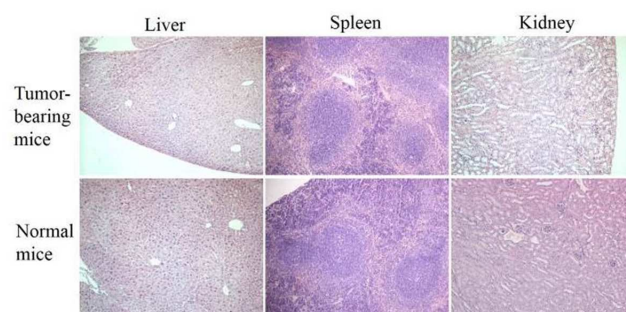


**Fig. 7.** Histopathologic analyses of H&E-stained tissue sections from the livers, spleens, and kidneys of tumor-bearing or normal mice injected with 0.1 mL 10 mmol/L  $\text{AuCl}_4^-$  solution prepared in PBS at 48 h post-injection. Appreciable pathological changes have not been found in all these organs.

Histopathological analysis was performed on the tissues obtained from the harvested organs (i.e., liver, spleen, and kidney) in this study. As seen in Fig. 7, images of H&E-stained tissue sections showed that no histopathological abnormalities or lesions were observed in the organs (i.e., liver, spleen, and kidney). Furthermore, no changes in eating, drinking, grooming, exploratory behavior, activity, physical features (e.g., weight and skin color), and neurological status were observed in HeLa tumor-bearing mice or normal mice injected with 0.1 mL 10 mmol/L  $\text{AuCl}_4^-$  solution prepared in PBS.

Based on the above observations, our studies illustrate that rapid and specific tumor targeting through specifically biosynthesized fluorescent gold nanoclusters could be readily realized by employing the peculiarities of cancer cells or tumor tissues

without any additional reducing agents, which could be utilized to efficiently and precisely bioimage regions of tumors *in vivo* and thus have enormous potential to improve the precision of cancer diagnostics and treatments. It is evident that the biosynthesized gold NCs and the systemic bio-administration process of gold precursors are biocompatible and have the ability to specifically target tumors and then locally active the biosynthesis of fluorescent NCs to broadcast tumor location *in vivo* (Fig. 2, Fig. 4 and Fig. 5). Meanwhile, the biosynthesized gold NCs reduced from the molecular precursor inside the cancerous cells keeps monodisperse without further aggregation and well distributed in target tumor cells, the resulting edges and morphologies of the cells neatly delineated with the good performance of the fluorescent nanoclusters (Fig. 4). Importantly, in addition to the targeting ability across multiple length scales in biological systems, the relevant fluorescence intensity increased with interaction /or incubation time (Fig. 4 and Fig. 5), indicating the capacity of the transportation and reduction of Au(III) salts to precisely induce accumulation and biosynthesis of fluorescent gold NCs in tumors to enhance *in vivo* diagnostics and therapeutics. Previously, we demonstrated that no nanocluster biosynthesis occurs in the normal cell controls under the conditions and time periods considered here, suggesting that the mechanism must stem from some specific biochemical characteristics of tumor cells which differentiate them from cells under normal homeostasis<sup>13</sup>. Reduction of the molecular precursor to fluorescent gold NCs inside the cancerous cells is presumably due to the reducing bio-agents and specific peculiarities of target cells, which allow the cells to control their inherent highly oxidized status<sup>20-23</sup>.

Having probed the high sensitivity and specific tumor targeting effect through biosynthesized fluorescent gold NCs in tumors, we next investigated whether these tumor-targeted gold NCs could effectively specify tumour tissues and precisely bioimage several tumors simultaneously occurring in mice. As shown in Fig. 5 I, when the molecular precursor Au(III) salts were intravenously administered to blank mouse model or mice bearing HeLa carcinoma tumors, the *in vivo* tumor targeting images demonstrate that the fluorescent gold NCs can be spontaneously and selectively biosynthesized in tumor tissues, and the special microenvironment of tumor owns its particularity from normal tissues/organs which can help to readily reduce  $\text{Au}^{3+}$  to the state of fluorescent gold NCs, evidencing the ability of rapid and specific tumor targeting through biosynthesized fluorescent nanoclusters in tumors to efficiently and precisely bioimage regions of tumors *in vivo*. Most interestingly, the fluorescence signal can be observed in urethra at 48 h, indicating that these gold species, ultrasmall fluorescent gold NCs, can be metabolized and cleared from the body through kidney filtration, which is consistent with the renal-clearable ultra-small gold nanoparticles Zheng's group reported<sup>11</sup>. Additionally, the result of histopathological analysis indicated that the gold NCs and the process of the gold precursor systemic bio-administration possess the good biocompatibility and bio-safety at animal level, despite the relatively high uptake in the organs (i.e., liver, spleen, and kidney) at 48 h. All these results suggest that the strategy of specific tumor targeting image by the biosynthesized gold NCs possesses availability and biosafety for promising biomedical

applications.

The uptakes of gold species on tumor tissues, as shown in Fig. 6, are generally well in consistency with the relevant imaging observed in Fig. 5, suggesting that the gold species prefer to accumulate on tumor tissues due to the particularity of tumor tissues or tumor microenvironments. It is evident that this particularity of tumor is facile to reduce  $\text{Au}^{3+}$  to the state of fluorescent gold NCs and makes the gold NCs in tumor tissues with a long retention time. The results of gold content biodistribution in different organs demonstrate that this gold species can be metabolized and cleared from the body through kidney filtration,<sup>15</sup> and, moreover, the fluorescent gold NCs for tumor targeting image can only be produced and withheld in tumor tissues.

It should be also pointed out that the data shown in Fig. 6, as follow up results of the *in vivo* experiments, are far from complete for describing the pharmacokinetics of the new probe reported herein. However, since the imaging contrast index, is dependent on the ratio of the amount of gold NCs in the tumor to that in the normal tissue background, clearance of the species from normal tissues also plays a key role in contrast enhancement and rapid detection. The rapid and precise bio-imaging of the target tumors could be readily realized in less than 2h through the specifically biosynthesized gold NCs *in vivo* after the intravenous injection of gold precursors through the tail of mice, evidencing the ability of rapid and specific tumor targeting through *in vivo* biosynthesized fluorescent NCs to efficiently facilitate simultaneous and multisite bioimaging of the precise tumor regions. The fluorescence signal from urethra at 48 h (Fig. 5-I-C) and the biodistribution of gold content (Fig. 6) indicate that these gold species, ultrasmall fluorescent gold NCs, prolong tumor retention, and meanwhile, can be metabolized and cleared from the body through kidney filtration. This tumor retention behavior coincides with that reported for PEG-coated gold nanoparticles<sup>24</sup>, exhibiting long tumor retention times due to the EPR effect. Therefore, this route could have more valuable potential in biomedical fields. But the current investigations have demonstrated that this strategy employing the biosynthesized gold NCs in tumor tissues is potentially useful for highly efficient tumor targeting *in vivo* image, as an alternative choice of fluorescent image contrast agents formed by the biosynthesized gold NCs in tumor tissues, at least for animal studies.

#### 4. Conclusions

In summary, we have developed a new strategy for highly efficient tumor targeting image by using specifically biosynthesized gold NCs in tumor tissues, which can exclude the side effects of direct injection of vectorized fluorescence nanoparticles or molecular fluorescence probes during the process of tumor diagnosis or identification. Our observations demonstrate that the *in vivo* biosynthesized gold NCs could produce tumor-specific accumulation of fluorescent NCs, highlighting the potential utilization for localizing the tumor's location and thus precisely imaging the disease affected regions with high spatiotemporal resolution. This may raise the possibility through the biosynthesized fluorescent gold NCs in tumors to pave a reliable way for exploring the *in vivo* applications of gold-based nano-species, especially in rapid tumor

targeting image, as a guide during surgical intervention for accurate tumor resection.

#### Notes

<sup>a</sup> State Key Laboratory of Bioelectronics (Chien-Shiung Wu Lab), School of Biological Science and Medical Engineering, Southeast University, Nanjing 210096, P. R. China. E-mail: [xuewang@seu.edu.cn](mailto:xuewang@seu.edu.cn).

<sup>b</sup> Ecole Normale Supérieure, UMR CNRS-ENS-UPMC 8640 and LIA CNRS XiamENS NanoBioChem Departement de Chimie, 24 rue Lhomond 75005 Paris (France)

<sup>c</sup> Daping Hospital, Third Military Medical University, Chongqing 400042, P. R. China

#### Acknowledgements

This work is supported by the National Basic Research Program (2010CB732404) and National Natural Science Foundation of China (81325011, 21327902) as well as National High Technology Research and Development Program of China (2012AA022703). In Paris this project is supported by UMR 8640 (ENS-CNRS-UPMC).

#### References

- 1 M. Zhu, C. M. Aikens, F. J. Hollander, G. C. Schatz and R. Jin, *J. Am. Chem. Soc.*, 2008, **130**, 5883–5885.
- 2 J. Zheng, P. R. Nicovich and R. M. Dickson, *Ann. Rev. Phys. Chem.*, 2007, **58**, 409–431.
- 3 Y. Kong, J. Chen, F. Gao, R. Brydson, B. Johnson, G. Heath, Y. Zhang, L. Wu and D. Zhou, *Nanoscale*, 2013, **5**, 1009–1017.
- 4 Y. Tao, Z. Li, E. Ju, J. Ren and X. Qu, *Nanoscale*, 2013, **5**, 6154–6160.
- 5 J. Forestier, *Ann. Rheum. Dis.*, 1949, **8**, 132–134.
- 6 A. J. Lehman, J. M. Esdaile, A. V. Klinkhoff, E. Grant, A. Fitzgerald and J. A. Canvin, *Arthritis Rheum.*, 2005, **52**, 1360–1370.
- 7 D. F. Yancey, S. T. Chill, L. Zhang, A. I. Frenkel, G. Henkelman and R. M. Crooks, *Chem. Sci.*, 2013, **4**, 2912–2921.
- 8 L. Shang, R. M. Dörllich, S. Brandholt, R. Schneider, V. Trouillet, M. Bruns, D. Gerthsen and G. U. Nienhaus, *Nanoscale*, 2011, **3**, 2009–2014.
- 9 C. Li, *Nat. Mat.*, 2014, **13**, 110–115.
- 10 X. Wu, X. He, K. Wang, C. Xie, B. Zhou and Z. Qing, *Nanoscale*, 2010, **2**, 2244–2249.
- 11 J. Liu, M. Yu, C. Zhou, S. Yang, X. Ning and J. Zheng, *J. Am. Chem. Soc.*, 2013, **135**, 4978–4981.
- 12 C. Zhou, M. Long, Y. Qin, X. Sun and J. Zheng, *Angew. Chem. Int. Ed.*, 2011, **50**, 3168–3172.
- 13 T. A. C. Kennedy, J. L. MacLean and J. Liu, *Chem. Commun.*, 2012, **48**, 6845–6847.
- 14 J. Xie, Y. Zheng and J. Y. Ying, *J. Am. Chem. Soc.*, 2009, **131**, 888–889.
- 15 X. D. Zhang, D. Wu, X. Shen, P. X. Liu, F. Y. Fan and S. J. Fan, *Biomaterials*, 2012, **33**, 4628–4638.
- 16 P. Priyabrata, A. Ahmad, D. Mandal, S. Senapati, S. R. Sainkar, M. I. Khan, R. Ramani, R. Parischa, P. V. Ajayakumar, M. Alam, M.

- Sastry and R. Kumar, *Angew. Chem. Int. Ed.*, 2001, **40**, 3585–3588.
- 17 I. Willner, R. Baron and B. Willner, *Adv. Mater.*, 2006, **18**, 1109–1120.
- 18 J. Wang, G. Zhang, Q. Li, H. Jiang, C. Liu, C. Amatore and X. Wang, *Sci. Rep.*, 2013, **3**, 1157.
- 19 C. Wang, J. Li, C. Amatore, Y. Chen, H. Jiang and X. Wang, *Angew. Chem. Int. Ed.* 2011, **50**, 11644–11648.
- 20 C. Amatore, S. Arbault, M. Guile and F. Lemaître, *Chem. Rev.*, 2008, **108**, 2585–2621.
- 21 H. Wiseman and B. Halliwell, *Biochem. J.*, 1996, **313**, 17–29.
- 22 D. Trachootham, J. Alexandre and P. Huang, *Nat. Rev. Drug Discov.*, 2009, **8**, 579–591.
- 23 G. P. Bienert, J. K. Schjoerring and T. P. Jahn, *Act. Biomembranes*, 2006, **1758**, 994–1003.
- 24 W. S. Cho, M. Cho, J. Jeong, M. Choi, H. Y. Cho, B. S. Han, S. H. Kim, H. O. Kim, Y. T. Lim, B. H. Chung and J. Jeong, *Toxicol. Appl. Pharmacol.* 2009, **236**, 16–24.